Unambiguous detection of OH and H_2O on the Moon from Chandrayaan-2 Imaging Infrared Spectrometer reflectance data using 3 μm hydration feature

Prakash Chauhan[1,*], Mamta Chauhan[1], Prabhakar A. Verma[1], Supriya Sharma[1], Satadru Bhattacharya[2], Aditya Kumar Dagar[2], Amitabh[2], Abhishek N. Patil[2], Ajay Kumar Parashar[2], Ankush Kumar[2], Nilesh Desai[2], Ritu Karidhal[3] and A. S. Kiran Kumar[4]

[1]Indian Institute of Remote Sensing, Indian Space Research Organization, Dehradun 248 001, India
[2]Space Applications Centre, Indian Space Research Organisation (ISRO), Ahmedabad 380 015, India
[3]U.R. Rao Satellite Centre, ISRO, Bengaluru 560 017, India
[4]Indian Space Research Organisation Head Quarters, Bengaluru 560 094, India

Imaging Infrared Spectrometer (IIRS) on-board Chandrayaan-2 is designed to measure lunar reflected and emitted solar radiation in 0.8–5.0 μm spectral range. Its high spatial resolution (~80 m) and extended spectral range is most suitable to completely characterize lunar hydration (2.8–3.5 μm region) attributed to the presence of OH and/or H_2O. Here we present initial results from IIRS reflectance data analysed to unambiguously detect and quantify lunar 3 μm absorption feature. After pre-processing and data-reduction, a physics based thermal correction analysis of IIRS reflectance spectra has been done using co-located temperature measurements. Hydration absorption was observed at all latitudes and surface types with varying degrees for all pixels in the study area and its absorption depth shows distinct variability associated with mineralogy, surface temperature and latitude.

Keywords: Imaging Infrared Spectrometer, lunar hydration, Moon, reflectance data, thermal correction.

UNTIL recently, the Earth's only natural satellite, viz. the Moon, was thought to be an anhydrous body and considered to be bone dry[1–3]. This view about the Moon changed with the remote sensing-based results obtained from Moon Mineralogy Mapper (M^3) data, a reflectance imaging spectrometer on-board India's first mission to the Moon, Chandrayaan-1 (ref. 4). M^3 has contributed immensely towards the detection of widely distributed hydration signatures across the Moon and at places, localized and more isolated occurrences using 3 μm spectral response[4–8]. The hydration was also observed from deep impact, Cassini, earth based telescopic observation and several other laboratory studies[9–11]. The hydration feature in the 2.8–3.5 μm spectral region of the electromagnetic spectrum (more commonly the '3 μm band') is due to the presence of hydroxyl (OH) groups attached to a metal cation or molecular water (H_2O), or a combination of the two. Remote detection of water and/or hydroxyl signatures on the lunar surface has acquired significant importance as it provides important clues to understand the various sources such as exogenous and endogenous origin and OH/H_2O production mechanism that have led to their detection on the lunar surface. Interpretation of radiance spectra of the Moon in the 3 μm region requires a thermal correction to lunar surface reflectance in non-polar regions owing to high daytime temperature of the Moon (often higher than 300 K), and contribution of thermally emitted radiance in the spectra beyond 2.5 μm (refs 12, 13). Improved algorithms have been developed to accurately account for thermal correction for M^3 data using realistic temperature estimates from Diviner data[14]. However, due to the limited spectral coverage of M^3, viz. only up to 3 μm, the exact nature of the observed hydration signatures could not be ascertained due to uncertainties associated with thermal correction. This made discrimination between OH and H_2O detection difficult and could not be accomplished using M^3 data[11]. It has been suggested that observations of the lunar surface at wavelengths beyond 3 μm greatly improve the removal of thermal emission[12]. It has been strongly recommended to have spectral bands up to 5 μm to implement thermal correction by simultaneously estimating the surface temperature of the Moon. Imaging Infrared Spectrometer (IIRS) on-board Ch-2, has been designed to cover an extended spectral range from 0.8 to 5 μm in order to understand the exact nature and accurate quantification of the observed lunar hydration. Since the successful launch of Ch-2, this

*For correspondence. (e-mail: prakash@iirs.gov.in)

spectrometer has been mapping the lunar surface at a spatial resolution of ~80 m in 256 spectrally contiguous channels from a circular orbit of 100 km (ref. 15). The primary objective of IIRS is to detect and map the lunar surface composition and volatiles to understand the origin and evolution of the Moon in a geologic context. Even though almost 95% of the lunar surface has been already mapped by Chandrayaan-1 M^3, IIRS having a relatively higher spatial and spectral resolution and an extended spectral range beyond 3 μm, will reassess the chemical make-up of the lunar crust and provide a global inventory of lunar hydration by discriminating OH, H_2O and water ice/ice frost in the polar regions. Specific science objectives of IIRS include identifying and mapping the lunar minerals and hydration feature. The spectral range of 2.5–3.5 μm is of utmost use for characterizing the hydration type, i.e. whether OH/H_2O/H_2O–ice is present in the lunar regolith and within the bedrock exposures of nominally anhydrous minerals all over the Moon as well as on the lunar poles. IIRS has been making systematic observations of the Moon since September 2019 from a circular orbit of 100 km over the lunar surface. Here we present initial results from Ch-2 IIRS hyperspectral data analysis to characterize lunar hydration at the 3 μm band and constrain thermal correction of lunar spectral reflectance between 2 and 5 μm. This orbital dataset from the Moon allows us to fully characterize the 3 μm absorption feature associated with OH and H_2O at relatively high spatial resolution. We quantify the lunar surface hydration (the sum of molecular water and hydroxyl group, known as 'total water') and provide an understanding for spatial distribution and linkages with mineralogy and surface temperature.

Data used

Ch-2 is Indian Space Research Organisation's (ISRO's) second mission to the Moon launched on 22 July 2019, with an orbiter, lander and rover for detailed analysis of lunar topography, mineralogy, surface chemistry, thermophysical characterization of the regolith and atmospheric composition. IIRS is one of payloads on-board Ch-2, which is placed in a 100 km polar orbit to acquire global scientific data. It is a grating-based dispersive instrument designed to measure reflected solar radiations and thermal emissions from the lunar surface in the spectral range 0.8–5 μm with spectral sampling of ~20 nm in 256 contiguous spectral bands[15]. Imaging with 80 m ground sampling distance and 20 km swath at nadir view from 100 km orbit altitude provides high-resolution spectral information to detect, characterize, quantify and map the lunar surface composition and volatiles, including hydration feature at 3 μm. Table 1 shows the major technical specifications of IIRS.

Table 1. Major specifications of Imaging Infrared Spectrometer payload on-board Chandrayaan-2

Parameters	Values
Payload platform attitude (km)	100
Spatial resolution (m) at nadir	80
Swath (km) at nadir	20
Spectral range (μm)	0.8–5.0
Spectral resolution (full width half maxima; nm)	~20
Noise equivalent differential radiance (NEdR; mW/cm^2/μm/sr)	≤0.005
No. of spectral bands	256
Quantization (bit)	14

The raw data collected from the IIRS payload were processed to correct the distortions present in them before being archived. Data processing for hyperspectral cubes of IIRS was done at three defined levels. Level-0 dataset consists of payload raw data (as they are collected from the payload), ancillary data (mainly SPICE kernels generated from the mission) and housekeeping data (health of the spacecraft). Level-1 data are radiometrically corrected, geometrically tagged and corrected for dark noise obtained before acquisition of each data strip. Level-1 dataset consists of processed radiance data (mW/cm^2/μm/sr) along with Seleno tagging in four different exposures and two different gain settings. The nominal data were acquired in exposure 1 (E1) and gain 2 (G2) settings. Spectral coverage of IIRS payload was achieved by joining four band-pass order sorting filters (OSFs) as part of the focal plane array joining around 1.2, 1.9 and 3.5 μm regions for achieving total spectral range.

Three strips of level-1 data collected during the first optical season were used for initial analysis for E1/G2 gain setting for three different dates, i.e. 16 June 2020 (strip-1), 12 June 2020 (strip-2) and 8 June 2020 (strip-3) respectively, and results have been presented. All the data strips selected for the analysis were from latitude range between 29°N and 62°N of the Moon, covering a broad range of geological settings in terms of lunar mare and highland regions. At the time of writing this article, IIRS coverage for the polar region beyond 62°N had not yet been acquired. The present study region has been previously shown to contain OH/H_2O (refs 4, 14). Figure 1 shows spatial coverage of these three data strips overlain on the global lunar reference image.

Methods

Spectrally and radiometrically calibrated level-1 IIRS spectral radiance data cubes were subjected to various data reductions, including per pixel lunar surface temperature estimation, thermal emission correction beyond 2 μm, conversion to apparent reflectance and empirical line correction for smoothing the observed reflectance spectra to detect 3 μm absorption caused by the presence of OH and H_2O, which could be further used to quantify water abundance. Figure 2 *a* shows the distribution of

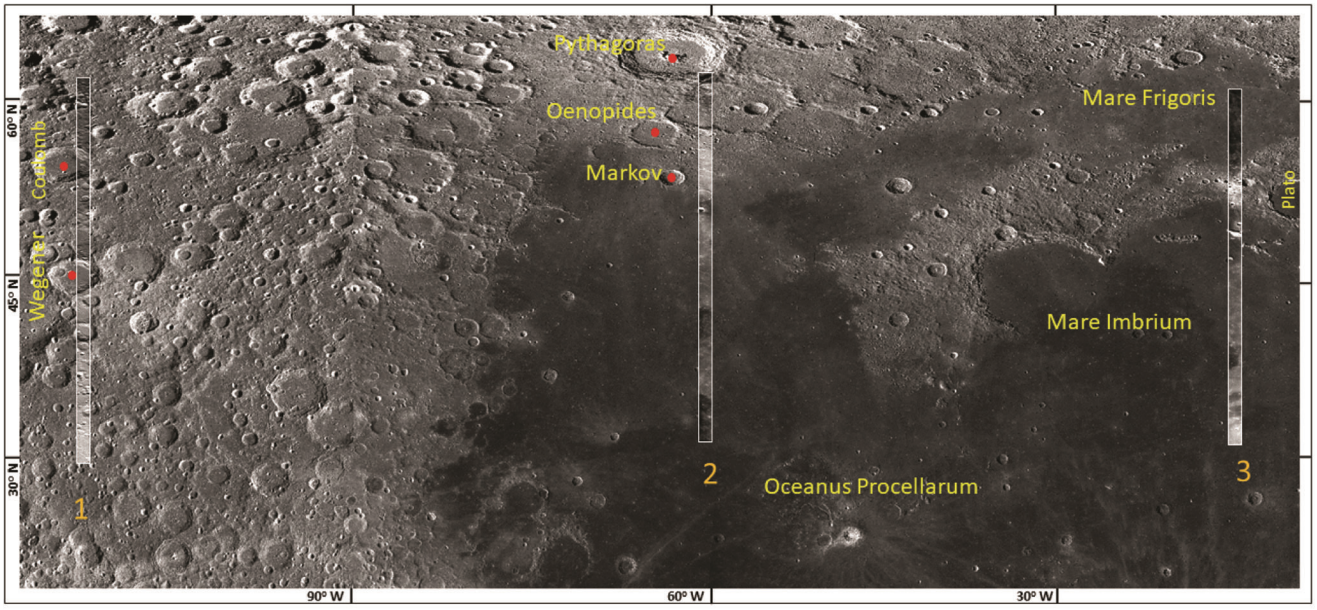

Figure 1. Chandrayaan-2 (Ch-2) Imaging Infrared Spectrometer (IIRS) data strips used in the present analysis overlain on LROC-WAC global mosaic to show their locations and geological context.

IIRS spectral radiance between 0.8 μm to 5 μm range, for selected pixels of data strip-2. Lunar spectra beyond 2 μm and below ~70° latitude were strongly affected by an additional component of thermally emitted radiance due to elevated surface temperature during sunlit conditions[13,16]. Relatively warmer pixels have higher radiance in the 4–5 μm range due to more thermal emission when compared to a cooler pixel.

Apparent reflectance conversion of IIRS spectral radiance data

The apparent spectral reflectance from measured spectral radiance dataset was calculated as follows[13]

$$R(\lambda) = \frac{\pi D^2 L(\lambda)}{F_0(\lambda)\cos(\theta)}, \quad (1)$$

where $L(\lambda)$ is the spectral radiance measured by IIRS, $F_0(\lambda)$ the incoming average solar flux on the lunar surface at 1 Å distance, D the mean Sun–Moon distance, θ the solar incidence angle on the lunar surface and λ is the wavelength.

$F_0(\lambda)$ was computed for spectral response for IIRS bands between 0.8 and 5 μm. Figure 2 *b* shows the latitudinal distribution of apparent spectral reflectance for the corresponding spectral radiance data shown in Figure 2 *a*. It can be clearly seen that spectral reflectance is dominated by thermal emittance beyond 2 μm and has strong latitudinal dependence as a function of lunar surface temperature.

Lunar surface temperature estimation and thermal emission correction

As discussed above, beyond about 2 μm, near-infrared spectra from the lunar surface contain a mixture of reflected sunlight and thermal emission caused by heating of the surface from the Sun. Such thermal emission complicates analysis of absorption features in the 3 μm and longer wavelength regions[16,17]. Accurate removal of thermal emission is vital for the study of the 3 μm feature and its variation in space and time. Different algorithms have been developed to remove thermal effect from reflectance imaging spectrometer datasets, mainly for the M^3 instrument[13,14]. Unlike the M^3 dataset which terminates at 3 μm wavelength range, IIRS spectral data have the advantage of simultaneous measurements of spectral radiance in the 4.5–4.9 μm range, recording purely emitted energy from the lunar surface. An algorithm has been developed to invert the lunar surface temperature using spectral radiance data in the 4.5–4.9 μm range. For each wavelength, radiance $L(\lambda)$, recorded by IIRS, is the sum of reflected solar irradiance and emission due to temperature of the surface given by eq. (2) below.

$$L(\lambda) = L_0(\lambda) + L_T(\lambda), \quad (2)$$

where $L_0(\lambda)$ is the reflected radiance, $L_T(\lambda)$ the thermal emission radiance by the surface temperature T, and $L_T(\lambda) = \varepsilon B(\lambda, T)$, where $B(\lambda, T)$ is Planck function at lunar surface temperature T (K), ε is the emissivity of the surface.

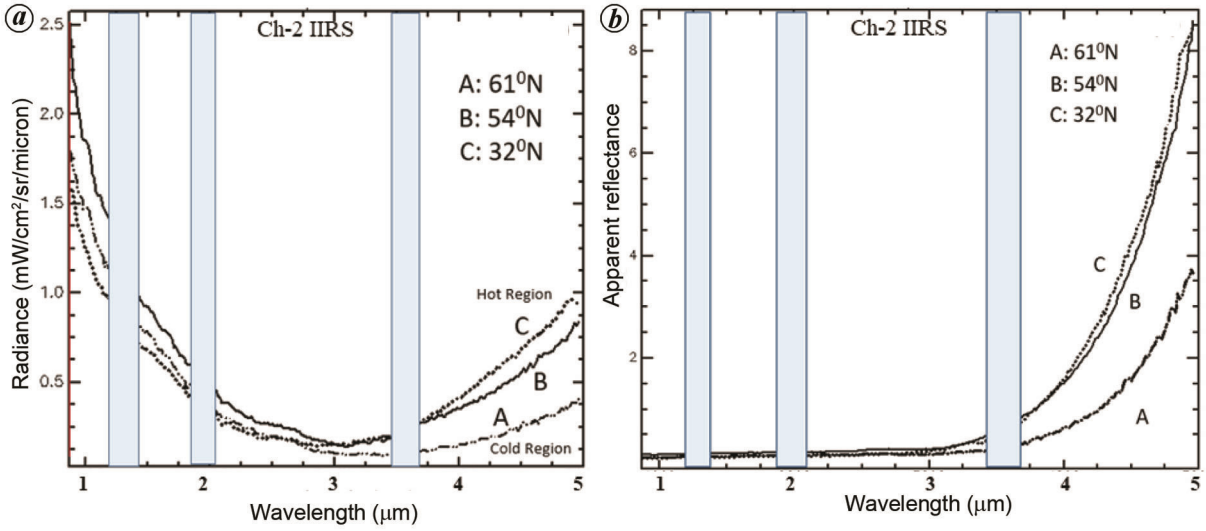

Figure 2. Per pixel latitudinal dependence of (***a***) spectral radiance and (***b***) apparent spectral reflectance as recorded for strip 2 by Ch-2 IIRS over the lunar surface. Thermal emission from the lunar surface from lower latitudes (C) dominates the spectra beyond 2.5 μm, compared to higher latitude regions (A). A relatively warm pixel shows higher radiance and reflectance values when compared to a relatively cold pixel. Vertical bars depict the location of order sorting filters for IIRS.

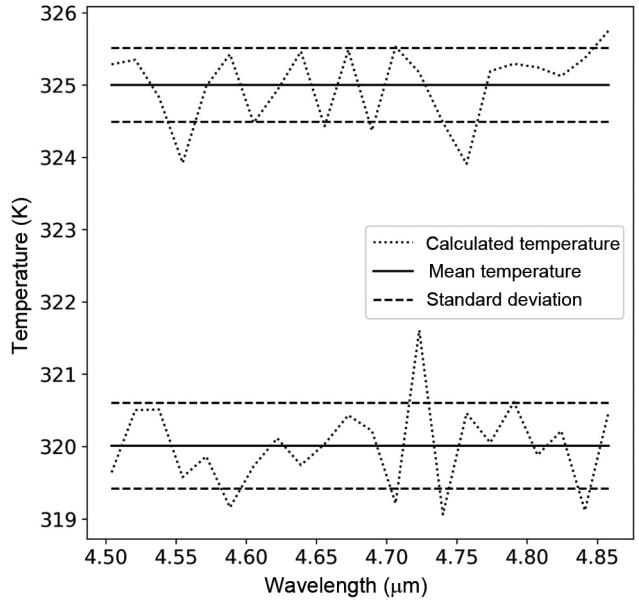

Figure 3. Lunar surface temperature values inverted for wavelength range between 4.5 and 4.9 μm for two representative pixels of IIRS data. Mean value is assigned as final temperature to the pixels of IIRS data. An uncertainty value of ± 0.5 K is observed for most of the retrievals for 0.95 lunar surface emissivity.

Incoming solar irradiance for wavelengths more than 4.5 μm is usually minimal compared to thermal emission, except for very cold surfaces and can be considered negligible. Hence, the solar component in apparent reflectance can be ignored and it can be assumed that radiance observed beyond 4.5 μm is only due to thermal emission. Many previous studies have suggested that an approximate emissivity value of 0.95 can be considered for the lunar surface and surface temperature for the pixels is calculated by inverting Planck's law[10]. With this assumption, the calculated temperature will have an uncertainty of ~3–4 K, due to assumed emissivity. Such small uncertainty in temperature will have negligible impact over reflectance values for thermal correction in the 2–3.5 μm spectral range. Using IIRS hyperspectral data, temperature values are inverted for different wavelengths between 4.5 and 4.9 μm, and a mean value is assigned as the final temperature to the pixel in question. It has been observed that in this wavelength region lunar surface temperature is more or less constant, as the lunar surface acts as an isothermal body. Figure 3 shows the retrieved surface temperature values between 4.5 and 4.9 μm spectral range for two representative pixels having different temperatures. Following this approach the lunar surface temperature for all three data strips was estimated. Figure 4 shows the estimated lunar surface temperature maps for the analysed IIRS data. Using the derived per pixel temperature values, thermal reflectance was calculated for 2–3.5 μm using Planck's law. Figure 5 shows the estimated thermal radiance and reflectance (I/F) values for different lunar surface temperature values. Using the eq. (3) below, the thermal corrected lunar surface reflectance values are obtained.

$$R_0(\lambda) = \frac{\pi D^2 (L(\lambda) - L_T(\lambda))}{F_0(\lambda)}, \tag{3}$$

where $R_0(\lambda)$ is the reflectance after removing thermal contribution between spectral range 0.8 and 3.5 μm. Figure 6 shows the result of thermal correction of IIRS spectra for different lunar temperature values and for different surface compositions.

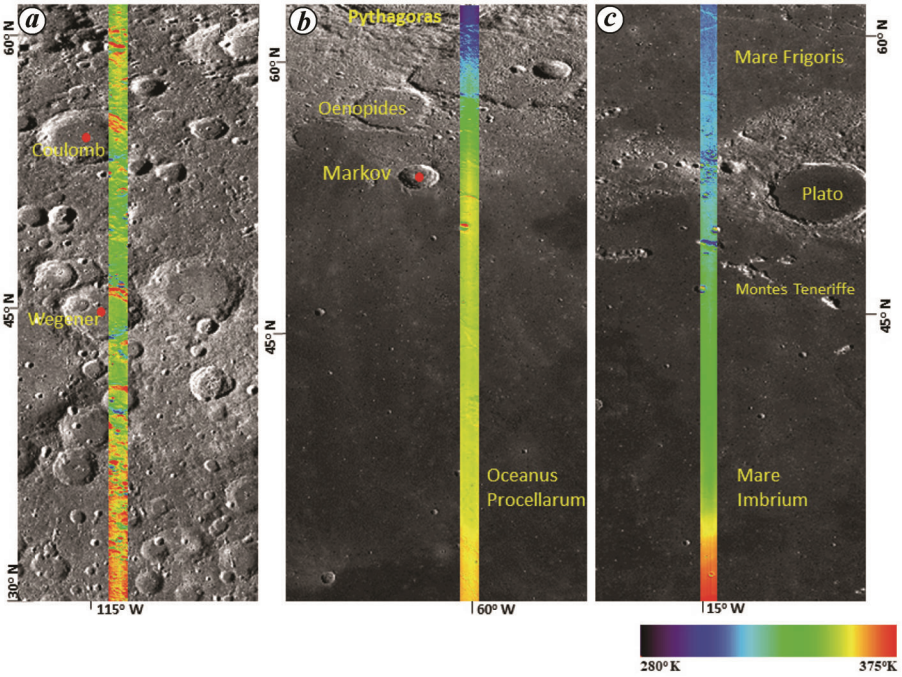

Figure 4. Lunar surface temperature maps for the three analysed strips generated from Ch-2 IIRS radiance data showing temperature distribution and its variation with latitude.

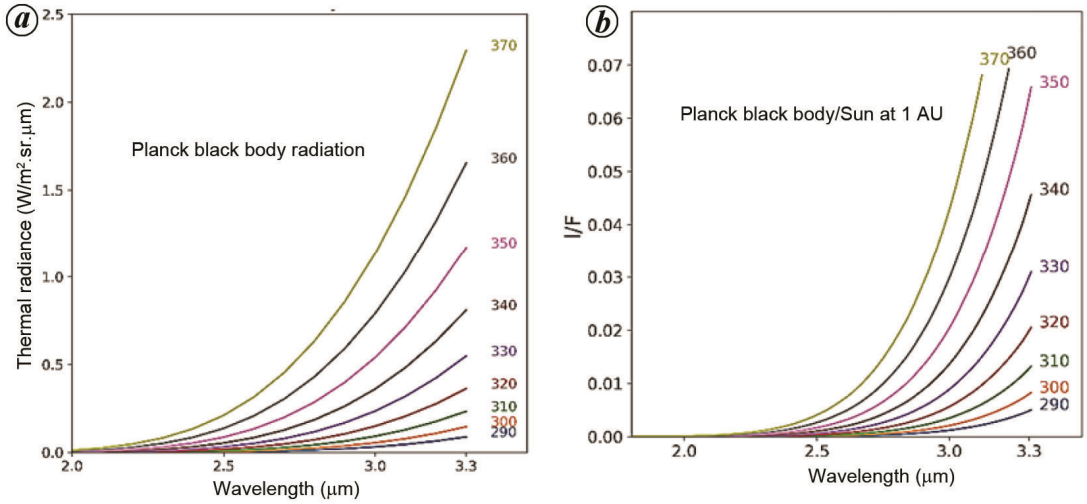

Figure 5. (***a***) Estimated thermal radiance and (***b***) reflectance (*I*/*F*) for different lunar surface temperature values (K).

Results

Detection of 3 μm OH and H_2O absorption in IIRS spectra

The hydration (OH and H_2O) absorption feature in IR spectra was characterized on the basis of the spectral absorption band in the 3 μm region distributed broadly from 2.7 to 3.5 μm (ref. 10). These features are spread across the Moon and have been detected from the bright sunlit portions and permanently-shadowed craters of the polar regions[18]. On the lunar surface such absorption is generally attributed to the presence of OH, but may indicate either distinct H_2O or water ice or a combination of both. These combinations of O–H stretching fundamentals and first overtone of 6 μm H–O–H bend, within the 3 μm region can be identified and separated only by sensors operating over the surface of the Moon with very high signal-to-noise ratio. Also, changes in the band positions arising due to differences in their crystal structure and nature of chemical associations make them spectrally different, for which interpretation is possible only with

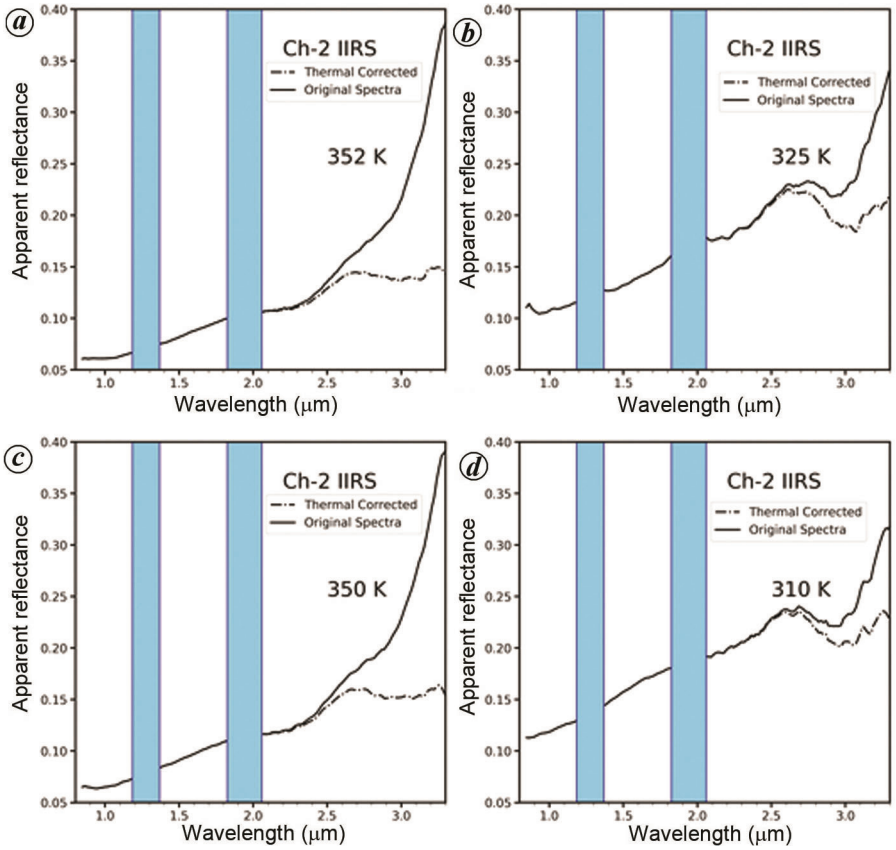

Figure 6. Reflectance spectra of Ch-2 IIRS data (strip-2) before (solid line) and after (dashed line) thermal correction for different lunar surface temperature values. ***a***, ***c***, For lunar mare surface with surface temperature of ~350 K showing no hydration feature at 3 μm. ***b***, For lunar plagioclase dominated region with surface temperature of 325 K. ***d***, For lunar highland regolith at 310 K showing a very strong lunar hydration feature at 3 μm.

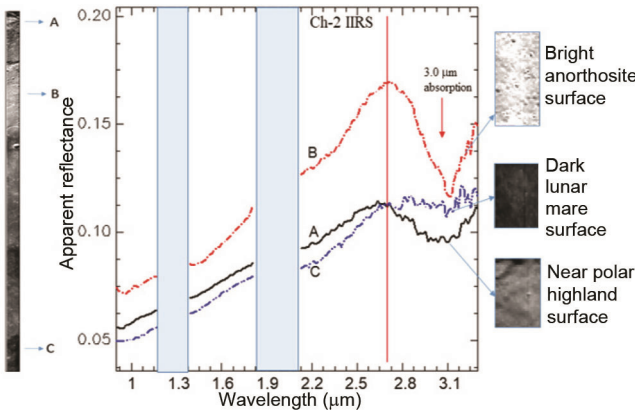

Figure 7. Thermally corrected lunar spectra for IIRS data strip-2 for bright anorthositic, mare and near-polar highland surfaces. It shows significant lunar hydration feature varying with different surface composition types.

high-resolution (both spectral and spatial) spectroscopic data.

Data strip-1 (lat. ~29–62°N and long. ~113–114°W) covers mostly the highland region passing through Coulomb and Wegner craters. Data strip-2 (lat. ~30–62°N and long. ~59–61°W) covers parts of the lunar surface starting from the edge of the Pythagoras crater and passing through the highland region and then covers the mare region. Data strip-3 (lat. ~29–61°N and long. ~14–16°W) starts from Mare Frigoris, passes through parts of Montes Teneriff region and covers Mare Imbrium. Data strips-2 and 3, lying in the mid-latitudes (between 29°N and 62°N) cover mostly the mare region however intermittent highland patches are also sampled. Figure 7 shows thermally corrected reflectance spectra from data strip-2 for different lithological units. It is clearly observed that plagioclase dominated surfaces have stronger absorption with steep slope and band centre around 3–3.08 μm. However, the high-latitude spectra of mature highland rocks around 61°E show relatively weak absorption, while lunar spectra of lower latitudes show a very weak absorption feature linked to lunar hydration.

Quantification of OH and H_2O on the lunar surface

The abundance of water and hydroxyl groups in the lunar and other geologic samples has been estimated traditionally using infrared absorption near 3 μm. Empirical

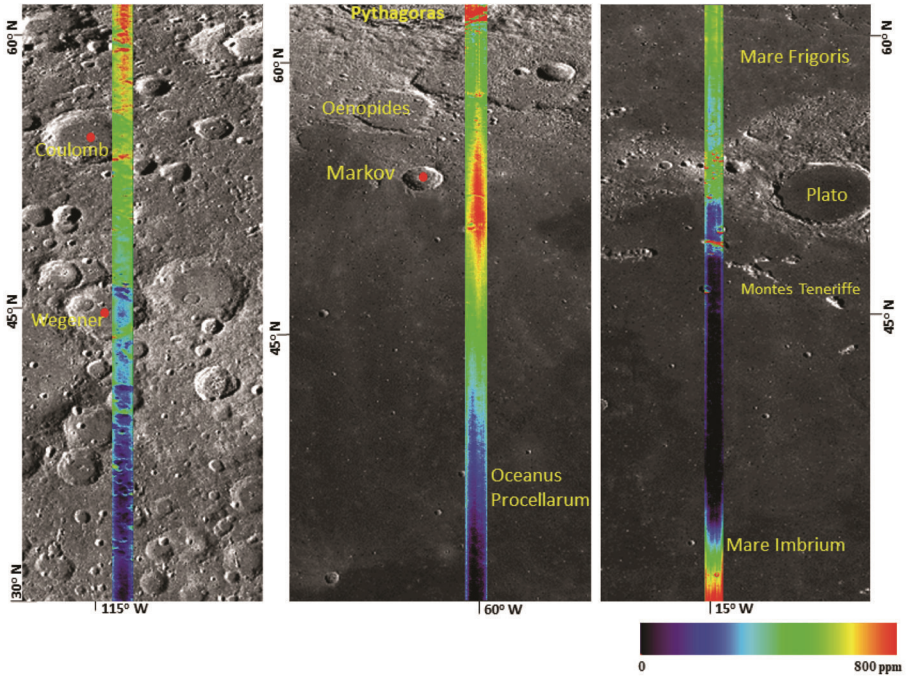

Figure 8. Total hydration maps for thermally corrected Ch-2 IIRS strips analysed in the present study. The observed total water concentration varies between near zero to 800 ppm having strong control on mineralogy and latitude.

relations are established between absorption data for water and hydroxyl groups and Beer's law is used to derive abundances. In the present study, spectra were acquired from regions representing lithological (mare, highland), latitudinal and topographical (slopes, rims, floor of the crater) variability, and analysed based on their band positions related directly to OH and H_2O abundance known as total water. In order to observe the spatial distribution of lunar hydration and map its concentration, hydration abundance maps were generated from the reflectance spectra. Empirical relationship for estimating the abundance of H_2O through remote sensing data has been developed and applied to the Moon using measurements of water-bearing glasses to calibrate M^3 data to water concentration[19,20]. To estimate the abundance of total water, the method proposed by Li and Milliken[20] has been used. Spectral parameter effective single-particle absorption thickness (ESPAT), which is linearly proportional to the abundance of total water has been used in this study. Thermally corrected reflectance data were converted to single scattering albedo (SSA)[21]. Later, continuum-removed SSA values were used to generate ESPAT parameter at 3 μm. After the calculation of ESPAT, water abundance (ppm H_2O) was estimated as follows[22]

$$H_2O \text{ ppm} = 0.8 * ESPAT_3 * 10{,}000. \quad (4)$$

Figure 8 presents the total hydration abundance maps for the three strips. The observed total water concentration was found to vary from near zero in lower-latitude mare regions to ~800 ppm in plagioclase-rich regions, suggesting strong control on mineralogy and latitudinal dependence.

Discussion

In the analysed strips, the enhanced hydration features were observed for brighter albedo regions with highland lithology and towards higher latitudes (Figure 8). The spectra from bright fresh regions and those associated with sunlit portion of craters showed a stronger absorption strength and more hydration (indicated by red colour), than seen in the mature mare portions (Figures 7 and 8). While the 2.8–2.86 μm absorption feature was more prominent in mare portion at warmer temperature (>320 K), the 3.0–3.05 μm absorption feature was present mostly at higher latitudes and for highland regions. The 2.8–2.86 μm feature was assigned specifically to the OH group, which is the most abundant form of hydration on the Moon. In the mare region with temperature more than 320 K, 2.8–2.86 μm absorption feature with shallow band depth was observed (Figure 7). This hydration feature also shows latitudinal variation with increase in band depth at higher latitudes, even for mare surfaces. The broader 3 μm absorption is the contribution of OH, but also with some H_2O which is formed as a by-product after the production of OH. It can also form when OH reaches close to its saturation[12]. The band position shifts to higher

wavelength after OH and H_2O get transported to the cold polar traps and are preserved there in relatively higher concentration[23]. The fine-grained and rough-textured property of lunar regolith provides significant surface area for adsorption of OH and H_2O to be detected even when their abundance is very less or single-layered[24].

The hydration feature in the lunar IR reflectance spectrum could be sourced from the surface by exogenic processes or can have an endogenic origin, i.e. mantle origin, or their combinations. Icy comets or water-bearing meteorites/asteroids are considered to have delivered OH and H_2O into the early Moon forming the source for lunar primordial water[25]. Hydrogen isotopic analysis and reported D/H values are also indicative of cometary input[26,27]. This primary magmatic water is introduced within silicate minerals (such as, nominally anhydrous minerals, fluid inclusions) and volcanic glasses by primary crystallization of magma, that in turn serve as their storehouse. Olivine melt inclusion, lunar picritic glass beads, and apatite, a common and late crystallized igneous mineral have also been reported to have significant concentration of water[28–30].

However, the most common and widespread process for the formation of OH and H_2O on the Moon is considered to be due to interaction of solar winds with the lunar surface[31,32]. This process is also termed as 'space weathering', which together with the micrometeoritic impacts form the most dominant surficial processes on the Moon. However, both processes act together in sourcing and producing the lunar OH and H_2O, as bombardment of lunar silicate and oxide-rich regolith surface with high-speed (300–800 m/s) charged particles of plasma (proton and electron) from solar wind[33] is accompanied by various physical and chemical changes[12,24]. In addition, the impact-induced comminution results in crushing and fracturing of the minerals present therein and produces irregular surface with physical breaking of bonds. As these processes occur in vacuum, they enhance the chemical reactivity of the regolith particles and produce unsatisfied chemical bonds at the surface, at the defects and dislocation portions[34]. These sites serve as a fertile platform for the adsorption and trapping of solar-wind proton to form OH and H_2O. Proton adsorption on the charged surfaces, defects and grain boundary interfaces may result either in loosely bound physiosorbed, or strongly bonded and more stable chemisorbed water[23,24] (Figure 9 *a*). Thus, if water is present, minerals with defects or terminal metal sites will initially and rapidly form chemisorbed OH on its surface by dissociate chemisorption[24]. Besides, surficial adsorption, trapping of a fraction of the incoming charged solar protons in the defects and dislocation sites of minerals also forms OH by bonding with oxygen. In contrast to surface adsorption, protons that are implanted internally ~10 s of nanometer into the surface are more stable[35–37]. These processes with continued deposition of charged solar protons eventually evolve to form H_2O in lunar regolith[35,38]. It is therefore the combination of both surface area and interior abundance of hydrogen that ultimately controls the depth and spectral position of the 3 μm feature.

As observed in Figure 10, the anorthositic highland terrain characteristically shows a longer wavelength spectral feature towards 3–3.08 μm compared with the mare regions at higher temperature, where 2.8–2.86 μm is prominent. It could indicate presence of molecular water or combined involvement of both OH and H_2O. Silicates with SiO_4 tetrahedron structural units have strong bonds with readily available defects (cation vacancies) that could serve as potential sites to be filled by adsorbing OH and H_2O. When compared to olivine (nesosilicates) and pyroxenes (inosilicates) that dominate the mare region, plagioclase feldspar from the highlands has a framework structure (tectosilicates; Figure 9 *b–d*) with large interstices for large cations, and presence of higher abundance of chemisorption sites/dangling bonds[4,24] consistent with their hydrous affinity. Also, the H_2O partition coefficient between olivine and melt is smaller when compared with plagioclase and melt[39]. So, the observed compositional effect with more spectral absorption or hydrous concentration for anorthite-bearing highlands materials pertains to its crystal structure and thermodynamic properties. The present results therefore suggest that on the Moon, OH in the mare material with higher temperature (>320 K) has an absorption near 2.8–2.86 μm, while that in anorthositic highland material has a band near 3–3.08 μm or possibly longer (Figure 10 *a* and *b*). The OH–metal bond in tectosilicates is also much stronger than in pyroxenes. This will strengthen the absorption band so that a similar amount of OH in anorthosite will result in a deeper band and shifted towards longer wavelength, compared to OH in mare. Spectral features diagnostic of H_2O also exist in the 3 μm region (e.g. near 3.1 μm due to H–O–H bend mode).

The increase of hydration absorption band depth with latitude has been suggested by previous studies to be controlled by temperature and is associated with stability of hydroxyl radical at low temperature[40]. Once, water molecules are formed by solar wind proton implantation, they undergo temperature-driven distribution through desorption and reabsorption process during local daytime. Around midday OH and H_2O are liberated through thermal desorption while in early afternoon, they are reabsorbed through recombinative desorption, as reported from LRO-LAMP observations[41]. Repeated breaking and reestablishment of bonds allow these volatile molecules to migrate and accumulate at higher latitude cold traps[24]. At lower latitudes due to high temperature (>300 K), desorption of OH and H_2O is higher[23,42] resulting in lower hydration. These observations are also consistent with results from satellites sensors, e.g. deep impact, Ch-1 M^3 and Lunar Prospector[4,10,43]. It has also been reported in previous studies that the mare regions have overall lower concentration of water than the highlands regions, which

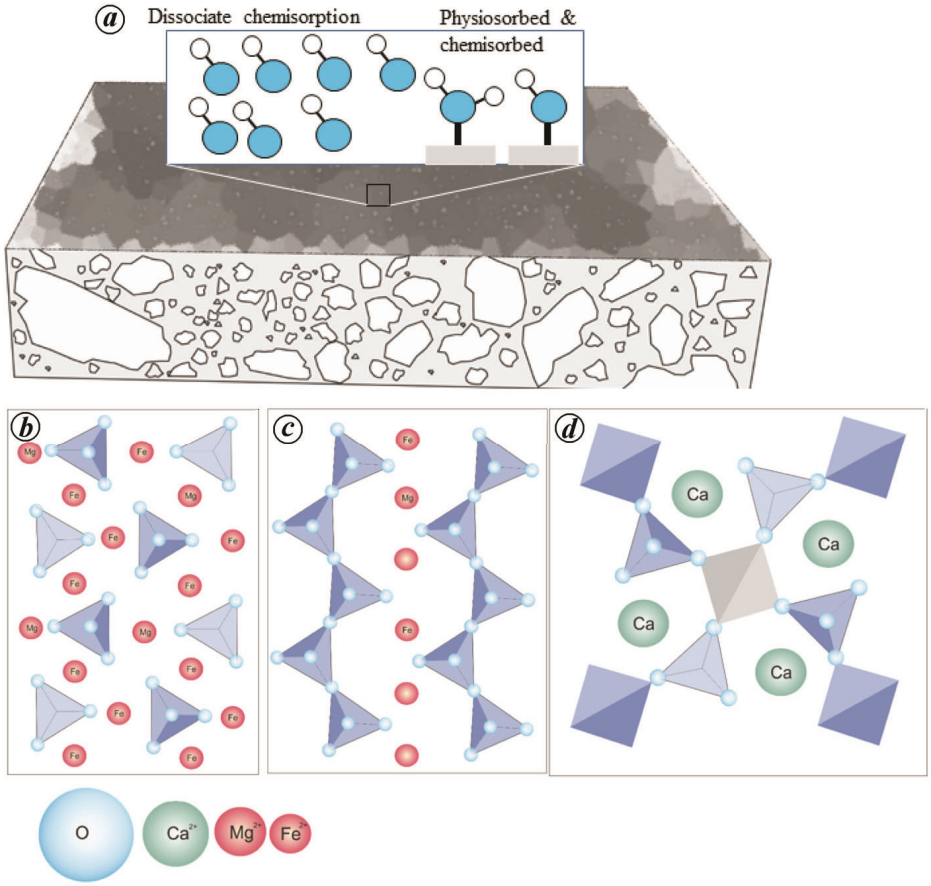

Figure 9. ***a***, Mode of occurrence of physiosorbed and chemisorbed water (OH/H_2O) on the lunar regolith. While the former one is loosely bound and likely to be diffused easily, the latter is bonded strongly by covalent bond with the mineral. Disassociate chemisorptions results in strong chemisorption of H_2O that results in the breaking of H–O–H bond, and its dissociation to OH. ***b–d***, Crystal structures of (***b***) olivine with isolated $(SiO_4)^{4-}$ tetrahedrons bounded by Fe and Mg cations, (***c***) pyroxenes with single-chained $(SiO_4)^{4-}$ tetrahedrons bounded by cation bands and (***d***) anorthite with $(SiO_4)^{4-}$ and $(AlO_4)^{4-}$ tetrahedrons arranged in 3D framework network with large cations accommodated in coordinated cavities.

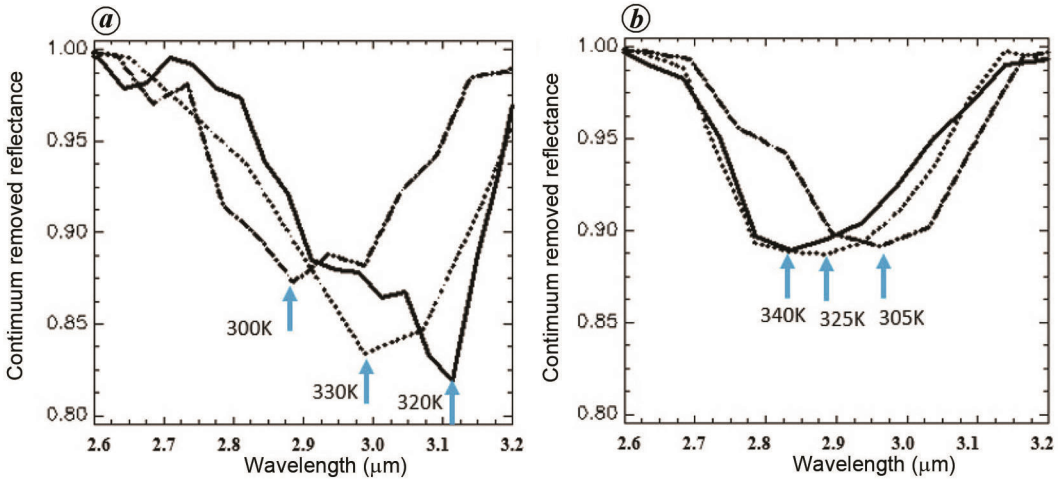

Figure 10. ***a***, Reflectance spectra from plagioclase-rich highland regions showing spectral shift of peak absorption for fresher surface towards longer wavelength up to 3.1 μm. Relatively bright surfaces show deeper hydration feature with not much of surface temperature control. ***b***, Reflectance spectra for mare surfaces showing spectral shift towards longer wavelength as a function of surface temperature. Cooler mare surfaces show peak absorption around 3 μm compared to warm mare regions having peak absorption around 2.8 μm. In general, plagioclase-dominated highlands have more hydration band strength.

may be due to lower overall number of activation sites and/or to lower binding energy for water on these grains[41].

From the above discussion and spatial distribution of IIRS spectra in the 3 μm band along with band depth centre that shifts from ~2.8 to longer wavelengths, even up to 3.1 μm over anorthositic highlands and over higher latitudes, we can interpret that Ch-2 IIRS thermally corrected reflectance spectra are suitable for unambiguous detection of OH and H_2O.

Conclusion

The proper interpretation of hydration feature through spectral analysis is significant as it provides important inputs regarding geology and geophysics of the mantle in terms of their mineralogy, chemical composition, rheology and solar–wind interaction. This is also significant for future planetary exploration for resource utilization. The thermal stability of these hydration features depends upon how they interact with one another, with the surface and their environment at particular temperature range and therefore provides important clues about their origin and evolution. Three strips from Ch-2 IIRS sensor have been analysed for hydration feature given its high-spectral range extending up to 5 μm. The initial data analysis from IIRS, clearly demonstrates the presence of widespread lunar hydration and unambiguous detection of OH and H_2O signatures on the Moon between 29°N and 62°N lat., after incorporating physics-based thermal correction to reflectance data. Plagioclase-rich rocks have been found to have higher OH or possibly H_2O molecules when compared to the mare regions, which were found to have more dominance of OH at higher surface temperature. As more data will be available for analysis in the future, a much better and complete picture of 3 μm spectral absorption will emerge, highlighting the temporal dynamics, and mineralogical and surface temperature control of hydration process on the Moon.

1. Papike, J. J., Taylor, L. and Simon, S., Lunar minerals. In *The Lunar Source Book* (eds Heiken, G. H. *et al.*), Cambridge University Press, Cambridge, UK, 1991, pp. 121–182.
2. Lucey, P. G. *et al*., Understanding the lunar surface and space–Moon interactions. *Rev. Min. Geochem*., 2006, **60**, 83–219.
3. Lucey, P. G., The poles of the Moon. *Elements*, 2009, **5**, 41–46.
4. Pieters, C. M. *et al*., Character and spatial distribution of OH/H_2O on the surface of the Moon seen by M^3 on Chandrayaan-1. *Science*, 2009, **326**, 568–572.
5. Bhattacharaya, S. *et al*., Endogenic water on the moon associated with the non-mare silicic volcanism: implications for hydrated lunar interior. *Curr. Sci*., 2013, **105**, 685–691.
6. Klima, R. *et al*., Remote detection of magmatic water in Bullialdus crater on the Moon. *Nature Geosci.*, 2013; http://dx.doi.org/10.1038/NGEO1909.
7. Chauhan, P. *et al*., Detection of OH/H_2O on the central peak of Jackson crater from Moon Mineralogical Mapper (M^3) data onboard Chandrayaan-1. In Lunar and Planetary Science Conference, The Woodlands, Texas, USA, abstr. 2072, 2014, vol. 45.
8. Bhattacharya, S. *et al*., Detection of hydroxyl-bearing exposures of possible magmatic origin on the central peak of crater Theophilus using Chandrayaan-1 Moon Mineralogy Mapper (M^3) data. *Icarus*, 2015, **260**, 167–173.
9. Clark, R. N., Detection of adsorbed water and hydroxyl on the Moon. *Science*, 2009, **326**, 562–564; doi:10.1126/science.1178105.
10. Sunshine, J. M. *et al.*, Temporal and spatial variability of lunar hydration as observed by the deep impact spacecraft. *Science*, 2009, **326**, 565–568; doi:10.1126/science.1179788.
11. Honniball, C. I. *et al*., Molecular water detected on the sunlit Moon by SOFIA. *Nature Astron*., 2020, **5**, 121–127; https://doi.org/10.1038/s41550-020-01222-x.
12. McCord, T. B. *et al*., Sources and physical processes responsible for the OH/H_2O in the lunar soil as revealed by the Moon Mineralogy Mapper (M^3). *J. Geophys. Res*., 2011, **116**, E00G05.
13. Clark, R. N. *et al*., Thermal removal from near-infrared imaging spectroscopy data of the Moon, *J. Geophys. Res*., 2011, **116**, E00G16; doi:10.1029/2010JE003751.
14. Li, S. and Milliken, R. E., An empirical thermal correction model for Moon Mineralogy Mapper data constrained by laboratory spectra and diviner temperatures. *J. Geophys. Res. Planets*, 2016, **121**, 2081–2107.
15. Chowdhury A. R. *et al*., Imaging infrared spectrometer onboard Chandrayaan-2 orbiter. *Curr. Sci*., 2020, **118(**3), 368–375.
16. Clark, R. N., Planetary reflectance measurements in the region of planetary thermal emission. *Icarus*, 1979, **40**, 94–103; doi: 10.1016/0019-1035(79)90056-3.
17. McCord, T. B. *et al*., Moon: near-infrared spectral reflectance, a first good look. *J. Geophys. Res*., 1981, **86**, 10883–10892.
18. Colaprete, A. *et al*., Water and more: an overview of LCROSS impact results. *Lunar Planet. Sci. Conf.*, abstr. Woodlands, Texas, 2335, 2010, vol. 41.
19. Milliken, R. E. and Mustard, J. F., Quantifying absolute water content of minerals using near-infrared reflectance spectroscopy. *J. Geophys. Res.*, 2005, **110**, E12001.
20. Li, S. and Milliken, R. E., Water on the surface of the Moon as seen by the Moon Mineralogy Mapper: distribution, abundance, and origins. *Sci. Adv*., 2017, **3**(9), e1701471.
21. Hapke, B., *Theory of Reflectance and Emittance Spectroscopy*, Cambridge University Press, New York, USA, 2012, 2nd edn, p. 513.
22. Honniball, C. I. *et al*., Telescopic observations of lunar hydration: variations and abundance. *J. Geophys. Res*., 2020, **125**, e2020JE006484l; https://doi.org/10.1029/2020JE006484.
23. Hibbitts, C. A. *et al*., Thermal stability of water and hydroxyl on the surface of the Moon from temperature-programmed desorption measurements of lunar analog materials. *Icarus*, 2011, **213**, 64–72.
24. Dyar, M. D., Hibbitts, C. A. and Orlando, T. M., Mechanisms for incorporation of hydrogen in and on terrestrial planetary surfaces. *Icarus*, 2010, **208**, 425–437.
25. Keays, R. K. *et al*., Trace elements and radioactivity in lunar rocks: implications for meteorite in fall, solar-wind flux, and formation conditions of Moon. *Science*, 1970, **167**, 490–493, doi:10.1126/science.167.3918.490.
26. Greenwood, J. P. *et al*., Hydrogen isotope ratios in lunar rocks indicate delivery of cometary water to the Moon. *Nature Geosci*., 2011, **4**, 79–82.
27. Saal, A. E., Hauri E. H., Van Orman J. A. and Rutherford, M. J., Hydrogen isotopes in lunar volcanic glasses and melt inclusions reveal a carbonaceous chondrite heritage. *Science*, 2013, **340**, 1317–1320.
28. Saal, A. E. *et al*., Volatile content of lunar volcanic glasses and the presence of water in the Moon's interior. *Nature*, 2008, **454**, 192–195.

29. Robinson, K. L. and Taylor, G. J., Heterogeneous distribution of water in the Moon. *Nature Geosci.*, 2014, **7**, 401–408; doi: 10.1038/NGEO2173.
30. McCubbin, F. M. *et al.*, Nominally hydrous magmatism on the Moon. *Proc. Natl. Acad. Sci. USA*, 2010, **107**, 11223–11228.
31. Hapke, B., Effects of simulated solar wind on the photometric properties of rock powders. *Ann. NY Acad. Sci.*, 1965, **123**, 711–721.
32. Starukhina, L., Water detection on atmosphere less celestial bodies: alternative explanations of the observations. *J. Geophys. Res.*, 2006, **106**, 14701–14710.
33. Smith, A. G., Radio Exploration of the Sun. D. Van Nostrand, Princeton, NJ, USA, 1967, p. 142.
34. Managadze, G. G. *et al.*, Simulating OH/H_2O formation by solar wind at the lunar surface. *Icarus*, 2011, **215**, 449–451.
35. Zeller, E. J., Ronca, L. B. and Levy, P. W., Proton-induced hydroxyl formation on the lunar surface. *J. Geophys. Res.*, 1966, **71**, 4855–4860.
36. Thiel, P. A. and Madey, T. E., The interaction of water with solid surfaces-fundamental-aspects. *Surf. Sci. Rep.*, 1987, **7**(6–8), 211–385.
37. Starukhina, L., Water detection on atmosphereless celestial bodies: alternative explanations of the observations, *J. Geophys. Res.*, 2001, **106**, 14701–14710; doi:10.1029/2000JE001307.
38. Farrell, W. M., Hurley, D. M. and Zimmerman, M. I., Solar wind implantation into lunar regolith: hydrogen retention in a surface with defects. *Icarus*, 2015, **255**, 116–126.
39. Hui, H., Peslier, A. H., Zhang, Y. and Neal, C. R., Water in lunar anorthosites and evidence for a wet early Moon. *Nature Geosci.*, 2013, **6**, 177–180; doi10.1038/ngeo1735.
40. Jones, B. M., Aleksandrov, A., Hibbitts, K., Dyar, M. D. and Orlando, T. M., Solar wind-induced water cycle on the Moon. *Geophys. Res. Lett.*, 2018, **45**, 10959–10967; https://doi.org/10.1029/2018GL080008.
41. Hendrix, A. R. *et al.*, Diurnally migrating lunar water: evidence from ultraviolet data. *Geophys. Res. Lett.*, 2019, **46**, 2417–2424; https://doi.org/10.1029/2018GL081821.
42. Poston, M. J. G. *et al.*, Temperature programmed desorption studies of water interactions with Apollo lunar samples 12001 and 72501. *Icarus*, 2015, **255**, 24–29; https://doi.org/10.1016/j.icarus.2014.09.049.
43. Feldman, W. C. *et al.*, Fluxes of fast and epithermal neutrons from lunar prospector: evidence for water ice at the lunar poles. *Science*, 1998, **281**, 1496–1500.

ACKNOWLEDGEMENTS. We thank Dr K. Sivan, Chairman, Indian Space Research Organisation/Secretary, DOS for encouragement while conducting lunar science studies, and ISRO's Chandrayaan-2 mission and ISSDC team for their continuous support for data collection, planning and archival support. We also thank the reviewers for their valuable suggestions that helped to improve the manuscript.

Received 15 March 2021; revised accepted 4 April 2021

doi: 10.18520/cs/v121/i3/391-401